Using hyperspectral imagery to predict post-wildfire soil water repellency

Sarah A. Lewis [a],*, Peter R. Robichaud [a], Bruce E. Frazier [b],
Joan Q. Wu [c], Denise Y.M. Laes [d]

[a] US Department of Agriculture, Forest Service, Rocky Mountain Research Station, 1221 S. Main Street, Moscow, ID 83843, USA
[b] Washington State University, Department of Crop and Soil Sciences, Pullman, WA 99164-6420, USA
[c] Washington State University, Department of Biological Systems Engineering, Pullman, WA 99164-6120, USA
[d] US Department of Agriculture, Forest Service, Remote Sensing Applications Center, 2222 W. 2300 S., Salt Lake City, UT 84119-2020, USA

Abstract

A principal task of evaluating large wildfires is to assess fire's effect on the soil in order to predict the potential watershed response. Two types of soil water repellency tests, the water drop penetration time (WDPT) test and the mini-disk infiltrometer (MDI) test, were performed after the Hayman Fire in Colorado, in the summer of 2002 to assess the infiltration potential of the soil. Remotely sensed hyperspectral imagery was also collected to map post-wildfire ground cover and soil condition. Detailed ground cover measurements were collected to validate the remotely sensed imagery and to examine the relationship between ground cover and soil water repellency. Percent ash cover measured on the ground was significantly correlated to WDPT ($r=0.42$; p-value<0.0001), and the MDI test ($r=-0.37$; p-value<0.0001). A Mixture Tuned Matched Filter (MTMF) spectral unmixing algorithm was applied to the hyperspectral imagery, which produced fractional cover maps of ash, soil, and scorched and green vegetation. The remotely sensed ash image had significant correlations to the water repellency tests, WDPT ($r=0.24$; p-value=0.001), and the MDI test ($r=-0.21$; p-value=0.005). An iterative threshold analysis was also applied to the ash and water repellency data to evaluate the relationship at increasingly higher levels of ash cover. Regression analysis between the means of grouped data: MDI time vs. ash cover data ($R^2=0.75$) and vs. Ash MTMF scores ($R^2=0.63$) yielded significantly stronger relationships. From these results we found on-the-ground ash cover greater than 49% and remotely sensed ash cover greater than 33% to be indicative of strongly water repellent soils. Combining these results with geostatistical analyses indicated a spatial autocorrelation range of 15 to 40 m. Image pixels with high ash cover (>33%), including pixels within 15 m of these pixel patches, were used to create a likelihood map of soil water repellency. This map is a good indicator of areas where soil experienced severe fire effects—areas that likely have strong water repellent soil conditions and higher potential for post-fire erosion.
Published by Elsevier B.V.

Keywords: Burn severity; Ash; Water repellent soils; Hayman Fire; Remote sensing

* Corresponding author. Tel.: +1 208 883 2346; fax: +1 208 883 2372.
  E-mail addresses: sarahlewis@fs.fed.us (S.A. Lewis),
probichaud@fs.fed.us (P.R. Robichaud), bfrazier@wsu.edu
(B.E. Frazier), jwu@wsu.edu (J.Q. Wu), dymlaes@fs.fed.us
(D.Y.M. Laes).

1. Introduction

Collecting timely information about soil conditions is among the most urgent and important tasks for

determining post-fire erosion potential and recommending mitigation measures. The hydrologic condition of soil changes considerably after a fire; water storage in the forest floor is lost, infiltration potential decreases, and runoff and erosion potentials increase (Robichaud, 2000; DeBano, 2000a; Letey, 2001). Much of the decrease in infiltration can be attributed to the formation of water repellent soils after a moderate or high severity fire (DeBano et al., 1976; Giovannini and Lucchesi, 1997; DeBano, 2000a).

Fires that have a long enough residence time (5–20 min) and reach high enough temperatures (175–280 °C) to completely volatilize the surface organic layer often render the soil water repellent (DeBano, 2000a; Robichaud and Hungerford, 2000; Shakesby et al., 2007). As the organic compounds cool in the deeper soil layers, they form a hydrophobic layer around individual soil particles (DeBano et al., 1976; Letey, 2001). The formation of this non-continuous hydrophobic layer generally occurs at or below the soil surface, up to 5 cm in depth (Clothier et al., 2000; DeBano, 2000b). Soil water repellency has high spatial variability; this non-continuity occurs laterally as well as vertically within the soil profile (Hallett et al., 2004; Taumer et al., 2005; Buczko et al., 2006; Woods et al., 2007). Laterally, the formation of water repellency is dependent on fluctuations in soil moisture, fuel loads, duff thickness, root holes, and micro-climatic conditions during combustion (DeBano, 2000a; Robichaud, 2000). Vertically, water repellency is generally dependent on the soil heat gradient of the fire; higher soil temperatures often lead to the deeper formation of water repellent soils. The degree of water repellency depends on the pre-fire conditions, especially soil moisture and available fuel, as both may dictate the temperatures reached through the soil profile (Campbell et al., 1995; Robichaud and Hungerford, 2000).

The extent, degree, and spatial distribution of soil water repellency are important factors to consider when evaluating post-fire runoff and erosion potential (Graber et al., 2006; Woods et al., 2007). Two field methods for determining soil water repellency involve measuring respectively: 1) water drop penetration time (WDPT) (DeBano, 1981); and 2) a relative infiltration rate by a mini-disk infiltrometer (MDI) (Decagon Devices Inc., 2003)[1]. The WDPT is a well-established test, whereas the MDI is a newer test, which has been found to correlate well to the WDPT (Lewis et al., 2006; Robichaud et al., in review). These tests require several seconds to several minutes to complete and must be repeated many times within an area of interest (DeBano, 1981; Letey et al., 2000). A goal and challenge with either test is to make the point measurements meaningful at the scale of a single watershed up to an entire wildfire area.

Wildfires often cover large areas (>25,000 ha) and the aforementioned tests are highly limited for identifying and classifying water repellency on these large fires. Further, because of the time required and subjectivity involved with the current water repellency tests, the need for an alternative to intensive manual sampling is evident. Remotely sensed measurements may be a substitute for or supplement to in situ samples, especially if the remote estimates of water repellency are proven to be accurate and reliable. These measurements, combined with meaningful statistical and spatial relationships to field samples, would allow for the evaluation and mapping of soil water repellency in less time. Ground samples would still be required to validate the remotely sensed data, but fewer samples would be necessary.

Hyperspectral remote sensors garner high-resolution data that can distinguish a range of features beyond the scope of traditional multi-spectral satellite broadband imagery and show promise for improving the direct measurement of post-fire features and conditions (van Wagtendonk et al., 2004; Robichaud et al., 2007). Aerial hyperspectral sensors provide imagery in contiguous, narrow bands of reflectance spectra ranging from the visible through the short-wave infrared (SWIR) range of the electromagnetic (EM) spectrum (wavelengths 400–2500 nm). The spectral and spatial resolution is sensor-dependent; spectral resolution can average 14–18 nm between wavebands and the spatial resolution (pixel size) can be as fine as 1–5 m (Earth Search Sciences Inc., 2005).

A single image pixel is the sum of the individual reflectance spectra from a mixture of surface materials (Theseira et al., 2003; Song, 2005). The characteristic features of the individual spectra from each reflective material within the image area are retained, and can be separated through spectral mixture modeling. Once these components are identified, linear unmixing of individual pixels can determine the fractional component spectra and, in turn, the fractional coverage of the surface materials being imaged (Adams et al., 1986; Roberts et al., 1993).

An inherent assumption in spectral mixture modeling is that pixels containing a single reflective material (a pure pixel) will be the best match to the input spectrum

---

[1] The use of trade or firm names in this publication is for reader information and does not imply endorsement by the U.S. Department of Agriculture or Washington State University of any product or service.

(Roberts et al., 1993). It follows that pixels with decreasing proportions of the target material will have a poorer chance of the target being correctly identified (Mundt et al., 2006; Glenn et al., 2005). Therefore, image classification and correlations to field data are expected to be most accurate and strongest in areas with abundant target materials.

Most land cover scenes can be mapped in spectral combinations of green vegetation, non-photosynthetic (senesced or scorched) vegetation, soil and shade (Roberts et al., 1993; Adams et al., 1995; Theseira et al., 2003; Song, 2005). A combination of these spectra along with an ash or char spectrum would account for the majority of the cover types of a typical post-fire scene. A previous investigation applied an unconstrained spectral unmixing model to hyperspectral imagery after the Hayman Fire to identify fractional cover of ash, soil,

charred and green vegetation (Robichaud et al., 2007). Significant correlations were found between the unmixing results and all related ground cover variables. A combination of ash and exposed mineral soil were found to be indicative of high soil burn severity. The ability to map post-fire ground characteristics at the sub-pixel scale presented a detailed and adequate assessment of the post-fire soil conditions.

The goal of this study was to examine the processed hyperspectral imagery from the Hayman Fire as a potential tool for determining post-fire soil water repellency. The specific objectives were: 1) to examine the correlations between ground measurements of water repellency and remotely sensed measures of ash, soil, scorched and green vegetation; 2) to examine the spatial relationship between ash cover and soil water repellency at the field plots; and 3) to use the spatial correlation
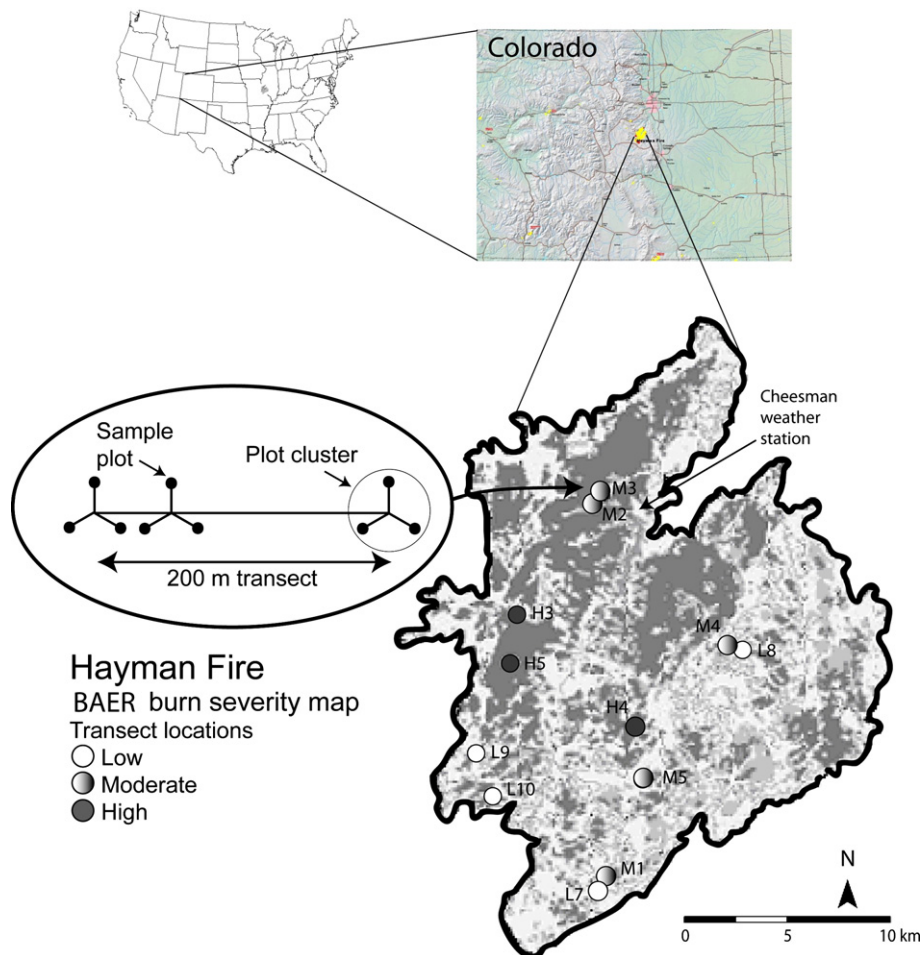

Fig. 1. Field site locations within the Hayman Fire overlaid on the BAER burn severity map. Sites were selected in low, moderate, and high burn severity. Also shown is an example transect layout, not to scale. One or two transects were located at each field site, with 4-m-diameter sample plots located on radials off the transects. The Cheesman weather station is shown for reference.

between ash cover and soil water repellency to create a map that indicates the likelihood of strong soil water repellency across the entire Hayman Fire area.

2. Study area

The Hayman Fire in Colorado was the chosen study area (approximately centered at 39°9′ N, 105°16′ W) (Fig. 1). In the summer of 2002, the Hayman Fire burned more than 55,000 ha within the South Platte River drainage on the Front Range of the Rocky Mountains, CO (Graham, 2003). The region is semi-arid, with a late summer monsoon season characterized by short-duration, high-intensity storms. The long-term average annual precipitation is 400 mm at the Cheesman weather station (39°13′ N, 105°17′ W, elevation 2100 m), with about 30% of the annual precipitation in July and August (WRCC, 2007; Finney et al., 2003). This region had experienced several years of drought, including 2002, and the accumulation of dry biomass was extensive (Finney et al., 2003). The region is underlain by the granitic Pikes Peak batholith, with frequent rock outcrops. The main soil types are Sphinx and Legault series, which are coarse-textured sandy loams, gravelly sandy loams and clay loams (Cipra et al., 2003; Robichaud et al., 2003). The dominant tree species are ponderosa pine (*Pinus ponderosa*) and Douglas-fir (*Pseudotsuga menziesii*) (Romme et al., 2003).

3. Research methods

An initial burn severity map of the Hayman Fire was created from a 16 June 2002 SPOT4 image (Robichaud et al., 2003; A. Parsons, pers. comm., 2005). This burn severity map was used by USDA Forest Service Burned Area Emergency Response (BAER) teams to guide post-fire rehabilitation, but within the scope of this project, the map was used only to guide field plot selection (Fig. 1). In Lewis et al. (2006) this BAER burn severity map was evaluated and found to be approximately 70% accurate compared to detailed field assessments of burn severity. In addition to its classification from the map, burn severity was also confirmed by visual evaluation. Areas burned at high severity were predominantly characterized by scorched and blackened vegetation and little remaining green vegetation, as well as extensive exposure of charred soil and ash. Moderately burned areas were characterized by a mix of green and scorched vegetation, and patches of charred soil and ash. Areas burned at low severity were differentiated by only light and fine fuel consumption and minimal charred soil exposure (Lewis et al., 2006).

3.1. Ground cover measurements

Ground reference field data were collected between 17 July and 2 August 2002. Approximately 60 sample plots were selected in each of the three burn severity classes as delineated by the BAER burn severity map and confirmed by visual assessment. At each of the 12 field sites, east–west transects were established in visually homogenous burn sites at least 20 m from roads. The location, number of plots, and burn severity class of each of the sites are in Table 1. The transects were designed to be 200 m in length (Fig. 1), with plot clusters at 0 m (west endpoint), 50 m, and 200 m (east endpoint). The locations of the center of each plot cluster were located with a GPS unit. At each of these

Table 1
Location of field sites, number of plots at each site, and the mean ash cover, water drop penetration time (WDPT) and mini-disk infiltrometer (MDI) time and rate at each site

Site	Number of plots	Burn severity	Latitude (N)	Longitude (W)	Ash (%)	WDPT (s)	MDI time (s)	MDI rate (ml min^{-1})
L7	18	Low	39°1′5.32″	105°18′9.07″	15	106	14	4.6
L8	15	Low	39°8′51.74″	105°12′29.23″	10	60	10	6.1
L9	15	Low	39°5′30.89″	105°23′21.99″	17	123	24	3.4
L10	15	Low	39°4′3.30″	105°22′30.54″	16	121	15	5.0
M1	9	Moderate	39°1′20.55″	105°18′2.07″	16	202	21	2.8
M2	9	Moderate	39°13′43.94″	105°18′3.35″	10	154	15	3.0
M3	9	Moderate	39°13′49.75″	105°18′14.01″	9	84	5	6.3
M4	15	Moderate	39°8′56.09″	105°12′46.53″	16	153	22	2.7
M5	18	Moderate	39°4′39.83″	105°16′29.89″	14	168	18	3.3
H3	18	High	39°9′59.68″	105°21′32.21″	20	98	18	5.6
H4	18	High	39°6′18.57″	105°16′48.38″	43	143	25	3.0
H5	24	High	39°8′21.96″	105°21′55.46″	10	87	22	4.8

center points, three 20-m radials were established at 0, 120 and 240°, respectively, with a tape and a compass. The sample plots were 4 m in diameter at the end of each of these radials.

The actual transect lengths were between 50 and 400 m, depending on topography and the uniformity of burn severity. In the low burn severity class, there were three 50-m transects with six plots each and five 200-m transects with nine plots each, for a total of 63 plots along eight transects. In the moderate burn severity class, there were six 200-m transects and one 50-m transect for a total of 60 sample plots along seven transects. In the high burn severity class, there were five 200-m transects and one 400-m transect for a total of 60 sample plots along six transects. The spatial and directional layout of the transects and sample plots was designed to encompass the spatial variability of the field measurements by sampling at short and long distances between sample plots (35 to 435 m apart) as well as sampling in different directions so that variation from slope position would be captured.

Fractional cover of all present ground cover components was visually estimated within the 4 m circle at each plot. Minor ground cover fractions, which were often grasses, forbs, shrubs, woody debris, or stumps were estimated first. A value of 1% was recorded if there was a trace of the material within the plot. The more abundant fractional ground cover components (exposed mineral soil and rock, ash, and litter) were then estimated with the largest cover component estimated last. All cover fractions summed to unity. Exposed mineral soil and rock were considered ground cover for the purpose of accounting for all space within a plot, and were combined into a single soil cover fraction. Percent green and percent char (scorch) of all ground cover (<1 m high) components were also calculated.

3.2. Soil water repellency tests

The WDPT test was performed every 5 cm along a 0.5-m line (11 measurements, including endpoints). Each test consisted of a water drop being placed on the soil surface and recording the time to complete infiltration. Soils were classified as water repellent when water drops remained on the soil surface for longer than 5 s (DeBano, 2000b; Letey et al., 2000). The degree of soil water repellency was assessed by measuring the persistence of the drop on the surface for up to 300 s. The median WDPT from each plot was used to divide the data into three classes based on the classification scheme of Dekker and Ritsema (1994): weak (5–60 s), moderate (61–180 s), and strong (181–300 s).

Four MDI tests were also completed at the same plots and within 0.5 m of the WDPT tests. The MDI (model Ml-1) maintains constant 5-mm suction and has a 31-m diameter porous disk through which the suction of the soil may break the tension across the plate and allow infiltration of water into the soil. The MDI was filled with water and placed on the soil surface. The time to the start of infiltration was noted (MDI time) up to 1 min, as well as the volume of water that infiltrated the soil within 1 min (MDI rate). Water repellency was divided into three classes, based on correspondence to the established WDPT classes, by the median MDI rate (Lewis et al., 2006; Robichaud et al., in review): weak (8 or more ml min^{-1}), moderate (4 to 7 ml min^{-1}), and strong (0 to 3 ml min^{-1}).

3.3. Aerial hyperspectral image acquisition and pre-processing

Fourteen adjacent flight lines of airborne hyperspectral imagery were collected on 10 August 2002 over the Hayman Fire between 1630 and 1900 UTC (solar noon 1905 UTC). The Probe I whisk-broom sensor was flown at 2100 m AGL and collected data along a track ~28 km long and 2.3 km wide—corresponding to a 512 pixel-wide swath with each pixel 5 m by 5 m at nadir. Reflected EM energy from the surface was received in 128 contiguous spectral bands that spanned 432 to 2512 nm, with a spectral bandwidth of 11 to 19 nm. A detailed description of data acquisition, atmospheric correction, and image processing can be found in Laes et al. (2004) and Robichaud et al. (2007).

The resulting georeferenced image was found to have registration errors of 5 to 10 m (1 to 2 pixels) after checking the location of about half of the transects relative to nearby road intersections. Where the flight lines overlap, up to 30 m (6 pixel) differences were visible. Fortunately, most of the ground plots did not fall in these overlap regions between flight lines. In order to compensate for some of this geolocational uncertainty, we used the GPS coordinates from the field plots, and averaged pixel values within a 5-m radius 'footprint' around each plot location in extracting the values for each sample plot.

3.4. Image analysis

The corrected image reflectance data were first reduced from 115 bands with the ENVI software minimum-noise-fraction (MNF) transformation to 20 MNF bands. The MNF transform estimated and then removed the noise from the data, resulting in a reduced

number of bands that contained the most meaningful information.

A library of image-derived spectra representing gray ash (a mixture of white ash and black char), bare soil, and scorched and green vegetation was created for each flight line for use in the unmixing process. The Pixel Purity Index (PPI) routine (Boardman, 1998) in ENVI software was used to identify the purest pixels, containing one homogenous cover type, in each flight line. By examining the spectral signature of each pixel and our a priori knowledge of most of the fire area we were able to select pixels in each flight line that represented ash, soil, scorched and green vegetation. The mean spectrum of several pure pixels in each class was calculated for use in the spectral unmixing. All libraries were transformed to MNF space using the same statistics file as derived from the MNF transformation of the corresponding flight line.

Mixture tuned matched filtering (MTMF) partial-unmixing algorithm (ENVI, 2004) was applied to the 20 MNF-transformed bands on all 14 flight lines of image data (Boardman, 1998). The MTMF score indicates how well the image pixel compares to the library reference spectra (ash, soil, scorched and green vegetation) and measures how spectrally abundant each material is in the image pixel. Spectral abundance in an image pixel corresponds to physical abundance in the same location on the ground. An MTMF score of zero means no match to the input endmember and no presence of the material in a pixel, while a score closer to one indicates a better match to the input endmember and greater abundance of the material in the pixel. The output of the MTMF routine was four MTMF score images: Ash MTMF, Soil MTMF, Scorch MTMF, and Green MTMF, along with an infeasibility (IF), or error, image. The IF value shows how likely or unlikely the match is. In general, pixels that combine higher MTMF scores with low IF values are a better match to the endmember spectrum. All MTMF score images were multiplied by 100 in order to assess the 1:1 correlations with the ground data. Individual fractional cover maps of each of the input

spectra were created in this process. Table 2 shows descriptive statistics of ground cover and MTMF scores by burn severity class.

3.5. Statistical analysis

The nonparametric Spearman rank correlation test (SAS Institute Inc., 2003) was used to assess the correlation between field measurements of water repellency and field and remotely sensed fractional ground cover measurements at the sample plot locations. Correlations were regarded significant at p-value < 0.05.

From previous work (Lewis et al., 2006), we knew a positive relationship existed between ash cover and water repellency—as ash cover increases, so does the strength and degree of water repellency. Since we were primarily interested in developing a relationship between ash and water repellency in areas at high risk for potential post-fire erosion (i.e. high ash cover or strong soil water repellency), we iteratively reduced the number of plots by eliminating the ones with the lowest ash cover (method further described by Mundt et al. (2006)). For example, in the first test, mean ash cover and mean MDI rate were calculated for all data, in the second test the means were calculated only for the data with greater than 0% ash cover, and in the third test for data with greater than 5% ash cover. This procedure was repeated at 5% increments up to 30% ash cover then at 10% increments up to 50% ash cover. A linear regression was applied to the means of these different groups, or bins, of data.

The spatial structure of soil water repellency occurrence was analyzed using the geoR package (Riberio and Diggle, 2001) in R (R Development Core Team, 2003). In general, spatial continuity means that two points close together will have more similar values than two points that are far apart (Isaaks and Srivastava, 1989). Empirical spherical semivariogram models (Eq. (1)) were created from the water repellency and ash measurements for each of the sites to identify the

Table 2
Means of measured ground cover and remotely sensed mixture tuned matched filter (MTMF) scores by burn severity class

	Ash	Ash	Soil	Soil	Scorched vegetation	Scorch	Green vegetation	Green
	(%)	MTMF	(%)	MTMF	(%)	MTMF	(%)	MTMF
Low severity $n=63$	15 (2.3)	4 (1.2)	27 (3.6)	3 (0.8)	60 (4.1)	19 (3.1)	19 (1.6)	11 (1.8)
Moderate severity $n=60$	13 (1.7)	11 (1.7)	39 (3.6)	1 (0.3)	45 (3.8)	17 (3.0)	7 (1.1)	3 (0.6)
High severity $n=60$	23 (3.0)	25 (4.3)	59 (3.4)	6 (0.9)	30 (2.2)	4 (1.5)	0 (1.2)	1 (0.2)

Standard errors are in parentheses.

Table 3
Spearman correlation coefficients (r) between water repellency measurements: water drop penetration time (WDPT) and mini-disk infiltrometer (MDI), the mean ground cover measurements, and the mean hyperspectral mixture tuned matched filter (MTMF) scores from the spectral unmixing results at all 183 field plot locations

	WDPT	MDI rate	MDI time
	(s)	(ml min^{-1})	(s)
Ground cover (%)			
Ash	**0.42 (<0.0001)**	**0.37 (<0.0001)**	**0.39 (<0.0001)**
Soil	**−0.22 (<0.0001)**	0.12 (0.10)	−0.10 (0.19)
Scorched vegetation	**0.16 (0.03)**	0.09 (0.24)	0.08 (0.29)
Green vegetation	**−0.16 (0.03)**	**0.22 (0.004)**	**−0.27 (0.0002)**
Matched filter (MTMF) scores			
Ash MTMF	**0.24 (0.001)**	**−0.21 (0.005)**	**0.22 (0.003)**
Soil MTMF	−0.11 (0.15)	0.23 (0.76)	0.03 (0.62)
Scorch MTMF	0.04 (0.56)	**−0.18 (0.02)**	**0.15 (0.03)**
Green MTMF	−0.05 (0.48)	0.13 (0.09)	−0.12 (0.09)

Bold correlations are significant at $p<0.05$ (p-values are in parentheses).

relationship between point pairs and their respective distance apart:

$$\gamma(h) = C_o + C\left(\frac{3h}{2a} - \frac{h^3}{2a^3}\right) \qquad (1)$$

This model estimates the semivariance (γ) between point pairs as the distance between points, or lag (h), approaches the practical distance, or range (a), at which estimations can be made between points (when $h \leq a$). The nugget (C_o) represents the discrepancy between zero and the model along the y-axis, and the partial sill (C) is the semivariance that can be predicted by the model. Beyond the range (when $h > a$), the value of the semivariogram is $C_o + C$. Semivariograms indicate both the variance between points and the range to which

the spatial relationship extends. Restricted Maximum Likelihood (REML) spherical models were fit to each semivariogram and a summary of the fit parameters was reported. A greater range indicates a greater distance of correlation between measurements, and a minimized $-\text{Log } L$ is a goodness of fit measure for the line fit to the data points on the semivariogram. Predictions can be reliably made between known points when the semivariogram model is a good fit, especially within the range of autocorrelation.

3.6. Map of soil water repellency

Based on the ash and water repellency threshold analysis and geostatistical analysis, a map of water repellent soils was created. The Ash MTMF score image was

Table 4
Iterative analysis with increasing ash cover on field plots

	Ash cover	Ash	WDPT	MDI time	MDI rate
	(%)	MTMF	(s)	(s)	(ml min^{-1})
All data ($n=183$)	17 (1.4)	13 (1.7)	121 (6.8)	18 (1.4)	4.3 (0.2)
Ash cover >0% ($n=165$)	19 (1.5)	14 (1.8)	128 (7.1)	19 (1.5)	4.1 (0.3)
Ash cover >5% ($n=112$)	26 (1.8)	18 (2.5)	148 (8.3)	24 (1.9)	3.4 (0.3)
Ash cover >10% ($n=79$)	33 (2.2)	20 (3.3)	155 (9.5)	25 (2.2)	3.4 (0.4)
Ash cover >15% ($n=68$)	35 (2.4)	21 (3.7)	164 (10.4)	26 (2.4)	3.2 (0.4)
Ash cover >20% ($n=42$)	45 (3.0)	27 (5.5)	155 (13.3)	27 (3.2)	3.3 (0.5)
Ash cover >25% ($n=38$)	47 (3.1)	28 (6.0)	169 (12.7)	30 (3.3)	2.4 (0.3)
Ash cover >30% ($n=24$)	57 (3.7)	37 (8.5)	159 (15.1)	26 (4.0)	2.7 (0.4)
Ash cover >40% ($n=16$)	66 (3.8)	44 (10.5)	155 (20.0)	23 (4.6)	2.9 (0.5)
Ash cover >50% ($n=11$)	74 (3.5)	55 (13.5)	180 (21.2)	29 (5.6)	2.4 (0.6)

Plots with the least amount of ash were eliminated in each iteration to examine the relationship between ash cover and water repellency in areas with abundant ash cover. The mean ash cover, ash mixture tuned matched filter (MTMF) score, water drop penetration time (WDPT) and mini-disk infiltrometer (MDI) time and rate are shown for each bin of data, standard errors are in parentheses.

limited to only include pixels with an MTMF score of at least 33. This value was found to be an indicator threshold for strongly water repellent soils. The range of autocorrelation between ash and water repellency measurements was used to create a buffer around these pixels to evaluate the likelihood of strongly water repellent soils occurring on or near pixels with significant ash cover.

4. Results

4.1. Correlation analysis

Ash was the fractional ground cover measurement that correlated most strongly with all three in situ water repellency measurements (Table 3). Correlation coefficients (r) ranged from -0.37 to 0.39 (p-value<0.0001)

for MDI rate and time to 0.42 (p-value<0.0001) for WDPT. A negative correlation with MDI rate and positive correlations with WDPT and MDI time indicate that as ash ground cover increased, so did the strength of soil water repellency. Green vegetation was also significantly correlated to all water repellency measurements (Table 3). Correlation coefficients ranged from ($r=-0.16$, p-value$=0.03$) for WDPT to ($r=-0.27$, p-value$=0.0002$) for MDI time and ($r=0.22$, p-value$=0.004$) for MDI rate. This relationship was opposite that of the relationship with ash; as green vegetation increased, the severity of the burn decreased, and the presence and strength of water repellency decreased.

The correlations between the Ash MTMF scores and the water repellency measurements were also statistically significant, WDPT ($r=0.24$, p-value$=0.001$), MDI
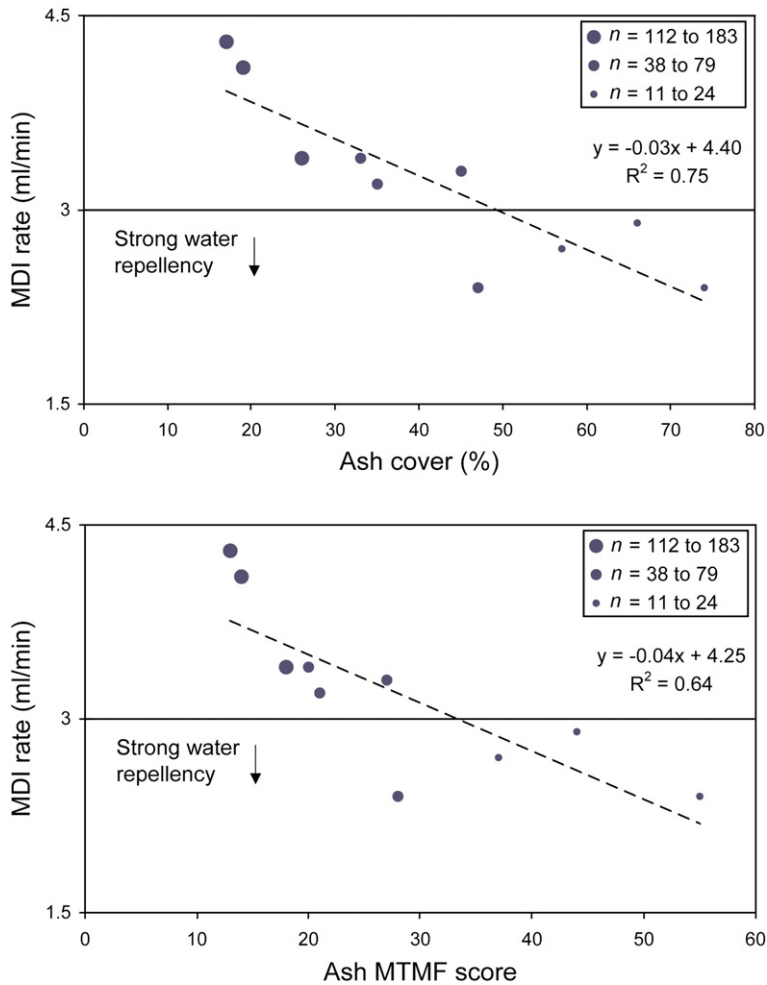

Fig. 2. Linear regression between the means of binned water repellency and ash cover plot data: a) MDI rate vs. ash cover (%), and b) MDI rate vs. Ash MTMF score. Note these graphs reflect a portion of the data presented in Table 4. As plots with low ash cover were eliminated, the n of each bin decreased, the mean ash cover on the plots increased, and the MDI rate values decreased. An MDI rate of 3 ml min^{-1} is the threshold for strong water repellency.

Table 5
Model fit parameters from the Restricted Maximum Likelihood (REML) spherical models fit to the empirical semivariograms at each of the field sites

Field variable	Model fit parameters	Field sites											
		Low burn severity				Moderate burn severity					High burn severity		
		L7	L8	L9	L10	M1	M2	M3	M4	M5	H3	H4	H5
Ash cover (%)	Partial sill (σ^2)	43	17	185	99	45	112	52	11	385	204	658	213
	Range (m)	14	17	51	14	36	86	57	13	36	50	49	35
	Nugget	494	152	0	289	0	0	0	143	0	0	0	0
	Log L	−78	−56	−56	−62	−26	−25	−27	−55	−75	−68	−78	−94
WDPT (s)	Partial sill (σ^2)	347	326	9612	5406	3916	1261	1796	14038	9269	9339	6581	1086
	Range (m)	12	16	31	200	98	15	16	92	35	36	31	11
	Nugget	5092	5876	0	2327	797	3873	6618	215	0	0	0	4223
	Log L	−97	−81	−84	−78	−44	−40	−48	−84	−102	−102	−99	−131
MDI time (s)	Partial sill (σ^2)	3	10	297	327	254	160	126	504	25	373	538	52
	Range (m)	12	17	20	38	120	40	56	107	15	50	19	60
	Nugget	202	182	78	0	0	0	0	92	288	0	0	364
	Log L	−69	−57	−61	−60	−31	−28	−30	−62	−73	−74	−78	−102
MDI rate (ml min^{-1})	Partial sill (σ^2)	9	0.5	6	14	9	5	2	5	0.25	23	3	14
	Range (m)	44	17	35	48	39	41	20	29	8	54	53	47
	Nugget	0	9	0	0	0	0	16	7	6	0	2	0
	Log L	−42	−36	−32	−38	−20	−16	−23	−31	−40	−50	−37	−62

The field variables used in the variogram analysis were ash cover, water drop penetration time (WDPT) and mini-disk infiltrometer (MDI) time and rate. A higher range indicates a greater distance of autocorrelation between measurements and a minimized Log likelihood (Log L) indicates a goodness of fit by the semivariogram model to the data.

time ($r = 0.22$, p-value = 0.003), and MDI rate ($r = -0.21$, p-value = 0.005) (Table 3). The only other MTMF scores that were statistically related to the water repellency measurements were from scorched vegetation (Scorch MTMF), MDI time ($r = 0.15$, p-value = 0.03) and MDI rate ($r = -0.18$, p-value = 0.02). Like ash, scorched vegetation is indicative of an area that burned.

4.2. Iterative threshold analysis

The relationship between ash cover and water repellency was further examined in areas with predominant ash cover. As expected, as ash cover increased, so did the degree of water repellency (Table 4). When examining all of the data, we found the mean ash cover on the plots was 17%, the mean WDPT was 121 s, the mean MDI rate was 4.3 ml min^{-1}, and the mean MDI time was 18 s. When this analysis was limited to only plots with ash cover greater than 50%, the mean ash cover increased to 74%, WDPT to 180 s, MDI rate decreased to 2.4 ml min^{-1}, and MDI time increased to 29 s (Table 4). Both water repellency tests indicate strong water repellency at this level of ash cover.

The data were binned in 5% increments of increasing ash cover, and the mean value of each bin was plotted to determine a threshold of ash cover that indicates strong water repellency (Fig. 2). An MDI rate below 3 ml min^{-1} is the threshold for strong water repellency (Lewis et al., 2006; Robichaud et al., in review). According to the

regression equation in Fig. 2a, when ash cover is greater than 49%, soils are likely to be strongly water repellent ($R^2 = 0.75$). A regression was also calculated between Ash MTMF score and MDI rate (Fig. 2b). From this equation, using the same MDI rate threshold of 3 ml min^{-1}, when the Ash MTMF score is greater than 33 (33% of a pixel is spectrally identified as ash), strongly water repellent soils are likely ($R^2 = 0.63$). In addition to the regression analysis shown in Fig. 2, regressions were also calculated between ash cover and WDPT ($R^2 = 0.62$) and MDI time ($R^2 = 0.43$), as well as Ash MTMF and WDPT ($R^2 = 0.53$) and MDI time ($R^2 = 0.32$).
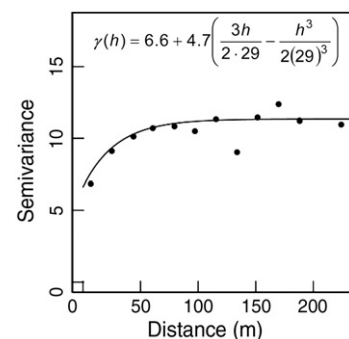

Fig. 3. Restricted Maximum Likelihood (REML) spherical model fit to an empirical semivariogram at moderate severity site M4 ($n = 15$). The range of spatial autocorrelation at this site between MDI rate measurements is 29 m, the nugget is 6.6 and the partial sill is 4.7.

4.3. Geostatistical analysis

Spatial relationships between water repellency measurements existed at the scale of 11 to 200 m (Table 5). An example variogram from moderate severity site, M4, is shown in Fig. 3. From the REML model-fit statistics, the range of spatial autocorrelation for the WDPT tests was between 11 and 200 m, with a mean of 49 m, while the ranges of autocorrelation for MDI time and MDI rate were 12 to 120 m (mean 46) and 8 to 48 m (mean 41),

respectively. The range of autocorrelation for ash cover was 13 to 86 m, with a mean of 38—these values were similar to the extent of values for the water repellency measurements. These results suggested that adjacent areas to the field plots would likely have similar water repellency characteristics, and that ash cover has a similar spatial structure compared to soil water repellency.

The ability to predict water repellency characteristics between known measurement locations enables us to
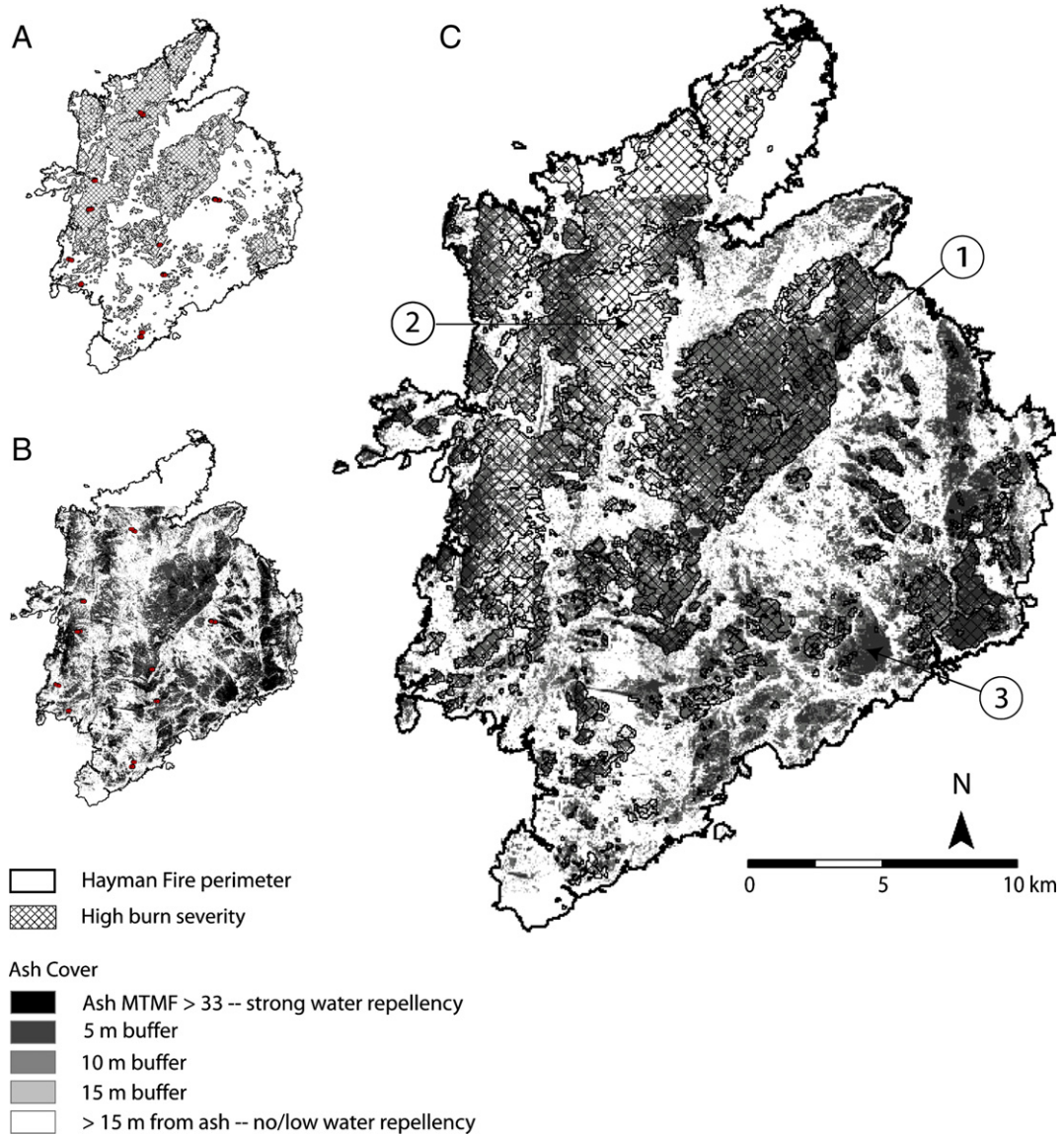

Fig. 4. Water repellency map of the Hayman Fire: A) high burn severity; B) high ash cover; and C) water repellency. Areas identified by the BAER team as high severity and areas with high ash cover are overlaid on this map. Area (1) is an example of a large patch of both high burn severity and high ash cover—these areas should be given high priority for evaluating runoff and erosion potential. Area (2) highlights a large area that was classified as high burn severity, whereas little ash was mapped. Area (3) shows a region with several patches of high ash cover that was not classified as high burn severity.

further examine the relationship between the ground measurements and the hyperspectral imagery. Given that the image pixels were 5 m, the minimum range of spatial autocorrelation of water repellency and ash cover at all sites was 10–15 m (2–3 image pixels), and the mean range was around 40 m (8 pixels), the adjacent pixels to the field plots in the imagery within the range of 15 to 40 m can be assumed to have similar water repellency measurements and ash cover. Within the range of spatial autocorrelation, measurements can be estimated between known points, allowing for comparisons across greater areas rather than between pairs of point measurements.

4.4. Map of soil water repellency

Fig. 4 presents probable areas of strong soil water repellency after the Hayman Fire. The black pixels have an Ash MTMF score of at least 33. The buffer around these pixels is a grayscale, with the next darkest pixels (dark gray) directly adjacent to a pixel with a high Ash MTMF score. The pixels get lighter as they are farther away from high Ash MTMF scores, with white representing areas greater than 15 m (3 pixels) away. Overlaid on this image are cross-hatched polygons representing high burn severity from the BAER map. Visually, there is a strong correspondence between the high Ash MTMF scores and high burn severity (Fig. 4C, area 1). However, there are large patches that were classified as high burn severity that did not map as ash in the imagery (Fig. 4C, area 2). Since post-fire rehabilitation treatments tend to focus on areas that are classified as high severity, these are areas that potentially were unnecessarily treated for erosion mitigation. Alternatively, there are areas that were mapped as high ash cover and were not classified as high burn severity (Fig. 4C, area 3). These areas, especially the larger patches of ash, are at risk for post-fire erosion, yet may have been overlooked by the BAER team because they were not classified as high burn severity.

The accuracy of this map was assessed using water repellency measurements from the field plots. The map was approximately 50% accurate for predicting strong water repellency directly from Ash MTMF scores. Of the 77 plots that exhibited strong water repellency based on the MDI rate (less than 3 ml min^{-1}), 35 were within 15 m of a pixel with high ash cover. Of the 55 plots classified as strong water repellency by the WDPT test (greater than 180 s), 31 were within 15 m of a pixel with high ash cover. Since the range of spatial autocorrelation averaged around 40 m for all field tests, a map was created by applying a buffer of eight pixels to the Ash MTMF image. The accuracy of this map was much

higher, 68 of the 77 plots (88%) were within 40 m of a pixel with high ash cover. This map was not shown because it did not correspond to the burn severity map very well and appeared to over-predicted ash cover and water repellency.

5. Discussion

Post-fire ash cover indicates complete or near-complete combustion of the pre-fire vegetation on the soil surface (Smith et al., 2005), which usually involves both high temperatures and long fire residence time. Thus, it is logical that ash covered the soils that were rendered most water repellent. This was the reasoning behind the threshold analysis—we were most concerned with the areas that had high ash cover, and not the areas with little or no ash cover. Subsetting the data to only include areas that had significant ash cover strengthened the relationship between ash cover and water repellency. As ash was more predominant on the plots, water repellency also increased. In our other work (Lewis et al., 2006; Robichaud et al., in review), we found MDI values less than 3 ml min^{-1} to be indicators of strongly water repellent soils and values greater than 3 ml min^{-1} to signify low or no water repellency. Although green vegetation was significantly (negatively) correlated to increasing water repellency, we did not focus on this relationship for two reasons. The relationship between green vegetation and water repellency was not as strong or statistically significant as with ash, and in a post-fire situation it is not the 'green' areas that are generally of interest when evaluating runoff and erosion potential. These areas are typically assumed to be at low risk for post-fire watershed response, and can naturally help mitigate runoff, erosion, and aid with fire recovery in general, if green areas exist within or surrounding severely burned areas.

A single pixel or plot with high ash cover or strong water repellency is not the cause for concern when considering post-fire erosion potential. Larger areas of adjacent pixels with high ash cover or strong water repellency, e.g. an entire hillslope, should be evaluated for erosion risk. In this study, our field sites covered an area of ~1 ha. One of our high severity sites (H4) had ash cover near 50% (Table 1). Four sites, M1, M2, M4, and H4 had mean MDI rates at or below 3 ml min^{-1}. These sites, especially H4, would be areas to investigate further for erosion and runoff potential.

Woods et al. (2007) suggested the importance of connectivity between patches of soil water repellency when predicting post-fire overland flow. They investigated the spatial variability of water repellency on the

scale of < 1 to > 100 m^2 and found water repellency to be patchy and variable at this scale. Variability at such a fine scale likely led to the spatial variability we measured at the greater ~1 ha scale. Woods et al. recommended sampling points for water repellency no closer than 1 m apart, and to sample areas larger than 100 m^2. We investigated spatial patterns in water repellency on the scale of 0.5 to 400 m and found that using geostatistics alone, we could predict between water repellency measurements up to about 40 m apart, but beyond that range we needed to incorporate a more continuous variable (ash cover) in our predictions. The correlation between ash cover and strong water repellency allowed for the creation of a likelihood map of water repellency across the entire Hayman Fire area. Woods et al. (2007) proposed that 35 to 75% water repellency on a site greater than 100 m^2 may induce overland flow. These numbers roughly correspond to our findings of greater than 33 to 50% ash cover on a site indicating strong water repellent soil conditions. Both studies generally indicate a need for attentiveness if more than one-third of a large area is covered in ash or strongly water repellent.

6. Limitations

Ideally, the hyperspectral imagery would have been acquired simultaneously with the field spectra and ground data, but smoke, weather, and logistical issues made a time delay unavoidable. The most likely changes in the ground conditions at the times that the ground data and imagery were collected are ash removal and char redistribution due to wind and rain, increased needlecast on the ground, and green revegetation, particularly near water sources. We were not able to quantify any of the changes at the plots. However, casual field observations during this time period and at the time of image acquisition suggested that changes in these conditions were minor and that the image captured the ground conditions at the time of ground data collection similar to the post-fire conditions. As with most remotely sensed imagery, canopy cover often occludes the soil surface, making ground to image correlations difficult. This was less of an issue in the areas burned at moderate and high severity, because there was little remaining canopy vegetation. Fortuitously, these were also the areas we were most interested in, because they had the most ash cover and water repellent soils.

There were some apparent registration problems with the imagery. These were most obvious near the edges of flight lines. However, most of our field sites did not fall in these regions. In order to compensate for some of the

error, we took a mean 'footprint' around each plot to better capture the conditions in the surrounding area and not just at a point location. The results from the geostatistical analysis also increased our confidence in the data because the minimum range of autocorrelation between measurements was 2–3 pixels. Even if our plot locations were off by a few meters due to mis-registration, they were likely representative of the actual location.

Geostatistical predictions based on a limited number of actual sample points can only be useful within a limited range of the samples. A stronger spatial autocorrelation allows for a more confident prediction over a greater area, but at the scale we are interested in (55,000 ha), the scale of autocorrelation between our measurements is not sufficient to use kriging techniques (Isaaks and Srivastava, 1989) to predict water repellency across the entire burned area. Instead we used Ash MTMF score, which was a continuous variable across the entire fire area, and created a buffer around these pixels based on the geostatistical range of autocorrelation with water repellency. This map was based on the distance to pixels with high ash cover—the closer to high ash cover (at least 33%), the higher the likelihood of strong water repellency. This map has limitations because it was based on modest correlations between point measurements of ash cover and soil water repellency that are extrapolated over the entire fire area. We were not able to directly map water repellent soils, so remotely sensed ash cover was used as an intermediate variable. Thus, we refer to this map as a likelihood map of soil water repellency, and only suggest that it be used in conjunction with other data as a guide for post-fire assessment.

A map of soil water repellency combined with burn severity, slope, aspect, soil, and other GIS layers would allow for a detailed examination of a burned area for post-fire erosion potential (Elliot et al., 2006). A map of the likelihood of water repellency over the entire fire area is a piece of information currently not available for BAER teams. However, the techniques presented here are not yet "rapid response" operational, and not available in the days immediately following a fire when post-fire rehabilitation treatment plans are made. As remote sensing technology advances and imagery becomes available more quickly and image processing is less laborious, these procedures and resulting products will provide detailed, useful information about post-fire soil conditions not previously available.

7. Conclusions

Immediate post-fire measurements of ground cover and water repellency indicated that ash cover, both measured

on the ground and remotely, was the variable most significantly correlated to strong water repellency after the Hayman Fire. Greater than 49% ash cover measured on the ground and 33% detected in the remotely sensed image indicated strongly water repellent soil conditions. Water repellent soils can greatly reduce post-fire infiltration potential, thus, areas with extensive ash cover should be examined closely for potential increased runoff and erosion. Based on a geostatistical analysis, spatial autocorrelation between ash cover and water repellency field measurements was found to exist on the scale of 15 to 40 m, which allowed for additional predictions between and beyond field plot locations. Remotely sensed ash cover was used as a continuous variable across the entire Hayman Fire to map patches of ash with at least 33% cover including areas within 15 m of these patches. The significant correlation between ash cover and soil water repellency allowed for mapping strong water repellent soil conditions. These results, combined with other information typically available in a post-fire situation, such as burn severity, soil characteristics, and slope, increase the ability to examine the potential for post-fire runoff and erosion. Further work is needed to improve the correlations between field and remotely sensed measurements, and to make high-resolution imagery available and easier to process within a few days immediately following a wildfire.

Acknowledgements

References

Adams, J.B., Smith, M.O., Johnson, P.E., 1986. Spectral mixture modeling: a new analysis of rock and soil types at the Viking Lander 1 site. Journal of Geophysical Research 91 (B8), 8098–8112.

Adams, J.B., Sabol, D.E., Kapos, V., Filho, R.A., Roberts, D.A., Smith, M.O., Gillespie, A.R., 1995. Classification of multispectral images based on fractions of endmembers: application to land-cover change in the Brazilian Amazon. Remote Sensing of Environment 52, 137–154.

Boardman, J.W., 1998. Leveraging the high dimensionality of AVIRIS data for improved subpixel target unmixing and rejection of false positives: mixture tuned matched filtering. In: Green, R.O. (Ed.), Summaries of the Seventh Annual JPL Airborne Earth Science Workshop, 12−16 January 1988, Pasadena, CA, vol. 1. California Institute of Technology, Pasadena, CA, p. 55.

Buczko, U., Bens, O., Durner, W., 2006. Spatial and temporal variability of water repellency in a sandy soil contaminated with tar oil and heavy metals. Journal of Contaminant Hydrology 88, 249–268.

Campbell, G.S., Jungbauer Jr., J.D., Bristow, K.L., Hungerford, R.D., 1995. Soil temperature and water content beneath a surface fire. Soil Science 159 (6), 363–374.

Cipra, J.E., Kelly, E.F., MacDonald, L., Norman, J., 2003. Ecological effects of the Hayman Fire part 3: soil properties, erosion and implications for rehabilitation and aquatic ecosystems. In: Graham, R.T. (Ed.), Hayman Fire Case Study Analysis. Forest Service General Technical Report RMRS-GTR-114. US Department of Agriculture Forest Service, Rocky Mountain Research Station, Fort Collins, CO, pp. 204–219.

Clothier, B.E., Vogeler, I., Magesan, G.N., 2000. The breakdown of water repellency and solute transport through a hydrophobic soil. Journal of Hydrology 231–232, 255–264.

DeBano, L.F., 1981. Water repellent soils: a state of the art. Forest Service General Technical Report GTR-PSW-46. US Department of Agriculture Forest Service, Pacific Southwest Research Station, Berkeley, CA. 21 p.

DeBano, L.F., 2000a. The role of fire and soil heating on water repellency in wildland environments: a review. Journal of Hydrology 231–232, 195–206.

DeBano, L.F., 2000b. Water repellency in soils: a historical overview. Journal of Hydrology 231–232, 4–32.

DeBano, L.F., Savage, S.M., Hamilton, D.A., 1976. The transfer of heat and hydrophobic substances during burning. Soil Science Society of America Journal 40, 779–782.

Decagon Devices Inc., 2003. Decagon Biophysical Instruments: Mini-Disk Infiltrometers. Pullman, WA. http://www.decagon.com/instruments/infilt.html (3 April 2007).

Dekker, L.W., Ritsema, C.J., 1994. How water moves in a water repellent sandy soil 1. Potential and actual water repellency. Water Resources Research 30, 2507–2517.

Earth Search Sciences Inc., 2005. The PROBE-1 Hyperspectral Instrument. Earth Search Sciences Inc., Lakeside, MT. http://www.earthsearch.com/index.php?sp=10 (23 April 2007).

Elliot, W.J., Miller, I.S., Glaza, B.D., 2006. Using WEPP technology to predict erosion and runoff following wildfire. American Society of Agricultural and Biological Engineers (ASABE) Annual International Meeting Paper No. 068011, 9−12 July, Portland, OR. 12 p.

Envi Version 4.1, 2004. The Environment for Visualizing Images, Ver. 4.1. Research Systems, Inc., Boulder, CO. http://www.ittvis.com/envi/index.asp (23 April 2007).

Finney, M.A., Bartlette, R., Bradshaw, L., Close, K., Collins, B.M., Gleason, P., Hao, W.M., Langowski, P., McGinely, J., McHugh, C.W., Martinson, E., Omi, P.N., Shepperd, W., Zeller, K., 2003. Fire behavior, fuel treatments, and fire suppression on the Hayman Fire. In: Graham, R.T. (Ed.), Hayman Fire Case Study Analysis. Forest Service General Technical Report RMRS-GTR-114. US Department of Agriculture Forest Service, Rocky Mountain Research Station, Fort Collins, CO, pp. 33–180.

Giovannini, G., Lucchesi, S., 1997. Modifications in soil physico-chemical parameters by experimental fires at different intensities. Soil Science 162 (7), 479–486.

Glenn, N.F., Mundt, J.T., Weber, K.T., Prather, T.S., Lass, L.W., Pettingill, J., 2005. Hyperspectral data processing for repeat detection of small infestations of leafy spurge. Remote Sensing of Environment 95, 399–412.

Graber, E.R., Ben-Arie, O., Wallach, R., 2006. Effect of sample disturbance on soil water repellency determination in sandy soils. Geoderma 136, 11–19.

Graham, R.T. (Ed.), 2003. Hayman Fire Case Study. Forest Service General Technical Report RMRS-GTR-114. US Department of Agriculture Forest Service, Rocky Mountain Research Station, Fort Collins, CO. 404 p.

Hallett, P.D., Nunan, N., Douglas, J.T., Young, I.M., 2004. Millimeter-scale spatial variability in soil water sorptivity: scale, surface elevation, and subcritical repellency effects. Soil Science Society of America Journal 68, 352–358.

Isaaks, E.H., Srivastava, R.M., 1989. An Introduction to Applied Geostatistics. Oxford Universtiy Press, New York. 561 p.

Laes, D., Maus, P., Lewis, S., Robichaud, P., Kokaly, R., 2004. Postfire burn-severity classification of the Hayman Fire, CO: based on hyperspectral data. Remote Sensing Applications Center Project Report RSAC-0068-RPT1. US Department of Agriculture Forest Service, Remote Sensing Applications Center, Salt Lake City, UT. 29 p. http://forest.moscowfsl.wsu.edu/pubs/?Robichaud2004p.pdf (2 September 2005).

Letey, J., 2001. Causes and consequences of fire-induced soil water repellency. Hydrological Processes 15, 2867–2875.

Letey, J., Carrillo, M.L.K., Pang, X.P., 2000. Approaches to characterize the degree of water repellency. Journal of Hydrology 231–232, 61–65.

Lewis, S.A., Wu, J.Q., Robichaud, P.R., 2006. Assessing burn severity and comparing soil water repellency, Hayman Fire, Colorado. Hydrological Processes 20, 1–16.

Mundt, J.T., Glenn, N.F., Weber, K.T., Pettingill, J.A., 2006. Determining target detection limits and accuracy delineation using an incremental technique. Remote Sensing of Environment 105, 34–40.

R Development Core Team, 2003. R: a Language and Environment for Statistical Computing. R Foundation for Statistical Computing, Vienna. http://www.R-project.org (10 March 2007).

Riberio Jr., P.J., Diggle, P.J., 2001. geoR: a package for geostatistical analysis. R-News vol. 1 (No 2).

Roberts, D.A., Smith, M.O., Adams, J.B., 1993. Green vegetation, nonphotosynthetic vegetation and soils in AVIRIS data. Remote Sensing of Environment 44, 255–269.

Robichaud, P.R., 2000. Fire effects on infiltration rates after prescribed fire in Northern Rocky Mountain forests, USA. Journal of Hydrology 231–232, 220–229.

Robichaud, P.R., Hungerford, R.D., 2000. Water repellency by laboratory burning of four northern Rocky Mountain forest soils. Journal of Hydrology 231–232, 207–219.

Robichaud, P.R., Lewis, S.A., Laes, D.Y.M., Hudak, A.T., Kokaly, R.F., Zamudio, J.A., 2007. Postfire soil burn severity mapping with hyperspectral image unmixing. Remote Sensing of Environment 108, 467–480.

Robichaud, P.R., Lewis, S.A., Ashmun, L.E., in review. Using a mini disk infiltrometer to determine soil water repellency. US Department of Agriculture Forest Service, Rocky Mountain Research Station Technical Note.

Robichaud, P., MacDonald, L., Freeouf, J., Neary, D., Martin, D., Ashmun, L., 2003. Postfire rehabilitation of the Hayman Fire. In: Graham, R.T. (Ed.), Hayman Fire Case Study Analysis. Forest Service General Technical Report RMRS-GTR-114. US Department of Agriculture Forest Service, Rocky Mountain Research Station, Fort Collins, CO, pp. 293–313.

Romme, W.H., Veblen, T.T., Kaufmann, M.R., Sherriff, R., Regan, C.M., 2003. Ecological effects of the Hayman Fire part 1: Historical (Pre-1860) and current (1860 to 2002) fire regimes. In: Graham, R.T. (Ed.), Hayman Fire Case Study Analysis. Forest Service General Technical Report RMRS-GTR-114. US Department of Agriculture Forest Service, Rocky Mountain Research Station, Fort Collins, CO, pp. 181–195.

SAS Insititute Inc., 2003. SAS® 9.1 Help and Documentation. Statistical Analysis Systems (SAS) Institute Inc., Cary, NC.

Shakesby, R.A., Wallbrink, P.J., Doerr, S.H., English, P.M., Chafer, C.J., Humphreys, G.S., Blake, W.H., Tomkins, K.M., 2007. Distinctiveness of wildfire effects on soil erosion in south-east Australiah eucalypt forests assessed in a global context. Forest Ecology and Management 238, 347–364.

Smith, A.M.S., Wooster, M.J., Drake, N.A., Dipotso, F.M., Falkowski, M.J., Hudak, A.T., 2005. Testing the potential of multi-spectral remote sensing for retrospectively estimating fire severity in African Savannahs. Remote Sensing of Environment 97, 92–115.

Song, C., 2005. Spectral mixture analysis for subpixel vegetation fractions in the urban environment: how to incorporate endmember variability? Remote Sensing of Environment 95, 248–263.

Taumer, K., Stoffregen, H., Wessolek, G., 2005. Determination of repellency distribution using soil organic matter and water content. Geoderma 125, 107–115.

Theseira, M.A., Thomas, G., Taylor, J.C., Gemmell, F., Varjo, J., 2003. Sensitivity of mixture modeling to end-member selection. International Journal of Remote Sensing 24 (7), 1559–1575.

van Wagtendonk, J.W., Root, R., Key, C.H., 2004. Comparison of AVIRIS and Landsat ETM+ detection capabilities for burn severity. Remote Sensing of Environment 92, 397–408.

Western Regional Climate Center (WRCC), 2007. Colorado Climate Summaries. WRCC, Reno, NV. http://www.wrcc.dri.edu/summary/climsmco.html (23 April 2007).

Woods, S.W., Birkas, A., Ahl, R., 2007. Spatial variability of soil hydrophobicity after wildfires in Montana and Colorado. Geomorphology 86, 465–479.